Novel Self-Assembling Close-Packed Droplet Array at the Interface in Ternary Polymer Blends

Nick Virgilio, Carl Marc-Aurèle, and Basil D. Favis*

CREPEC, Department of Chemical Engineering, École Polytechnique de Montréal, Montréal, Québec, H3C 3A7, Canada

Received November 12, 2008; Revised Manuscript Received February 10, 2009

ABSTRACT: This paper reports, for the first time, on the self-assembly of polystyrene (PS) droplets into a perfectly segregated close-packed droplet array at a high-density polyethylene/polypropylene (HDPE/PP) interface during melt processing. Remarkably, even when highly concentrated at the interface, the PS remains in droplet form and does not coalesce into a uniform layer at the interface. This highly organized, Pickering-type emulsion microstructure is induced by the partial wetting of the HDPE/PP interface by the PS droplets. It is shown that the affinity of the PS droplets for the HDPE/PP interface can be controlled by the addition of a 1,4-hydrogenated styrene−(ethylene−butylene) (SEB) diblock copolymer. A focused ion beam/atomic force microscopy technique is used to show that, depending on the concentration of SEB copolymer, the PS droplets migrate from the PP side to the HDPE side of the HDPE/PP interface due to the selective location of the SEB copolymer at the HDPE/PS interface. The close-packed droplet array at the interface is accentuated during annealing due to a "sweep and grab" effect induced by the coarsening of the HDPE/PP cocontinuous microstructure. It is shown that this phenomenon of assembled droplets, as well as the migration of the droplets at the interface, can be thermodynamically predicted via spreading coefficient theory. The special case of interfacial coalescence of the PS droplets in these systems was also studied by varying the time of quiescent annealing. In the unmodified blend, the coalescence rate is significantly higher for the PS droplets located at the HDPE/PP interface compared to the ones in the bulk phases. The addition of 1% SEB copolymer results in an even higher coalescence rate early in the quiescent annealing procedure. However, coalescence rapidly decreases and falls to virtually zero after 60 min due to the saturation of the HDPE/PS interface by the SEB copolymer. It is shown that when interfacially modified PS droplets are located at the HDPE/PP interface, they also serve to completely stabilize the cocontinuous HDPE/PP network from further coalescence. This work opens new perspectives in generating novel complex microstructures in polymer blends.

1. Introduction

The tendency of a liquid drop to spontaneously spread on a solid or on a liquid surface of another component is a classical phenomenon in the physics of wetting. In the early 1920s, Harkins presented a thermodynamic explanation of this effect.[1,2] He demonstrated that a liquid spontaneously spreads on a surface, i.e., completely wets the surface, if the interfacial free energy of the resulting system decreases. He then conducted a series of experiments with different drop-surface pairs and showed that a spreading coefficient λ_{ikj} was a simple and useful mathematical expression capable of predicting the wetting characteristics of many systems:

$$\lambda_{ikj} = \gamma_{ij} - (\gamma_{ik} + \gamma_{jk}) \quad (1)$$

In Harkin's setup, the γ's are the three interfacial tensions between the different pairs of materials, namely $\gamma_{\text{surface−atmosphere}}$, $\gamma_{\text{liquid−atmosphere}}$, and $\gamma_{\text{liquid−surface}}$. λ_{ikj} gives the tendency of component k (the liquid) to spontaneously spread at the interface of components i (in this case the surface) and j (the atmosphere). In order for component k to spread at the ij interface, the λ_{ikj} spreading coefficient must be positive. If negative, the spreading of k at the ij interface does not occur, or, in other words, component k does not wet the ij interface. It is worthy to note that in Harkin's original paper, the spreading coefficients had only two indexes, since the third (and omitted one j) was by default the atmosphere.

Subsequently, Torza and Mason[3] used this approach and generalized it for emulsions of three immiscible components. By considering the thermodynamic framework developed by Harkins, they showed that the resulting morphology of a ternary mixture can be predicted by using a set of three spreading coefficients, each giving the tendency of one component to spread at the interface of the other two. In ternary immiscible mixtures with constituents A, B, and C, the three spreading coefficients are calculated by successively designating components A, B, and C as the component k that spreads at the interface of the other two components i and j. Depending on the values of the three spreading coefficients, four different morphologies can result in blends composed of two major phases and one minor phase (Figure 1).

Three of these correspond to complete wetting (Figure 1a−c): two are complete segregation of the minor phase into the major phases and the third corresponds to spreading of the minor phase at the interface of the two major ones. The fourth morphology is the case of partial wetting.[3−5] In that case, none of the three components spreads at the interface of the other two. Instead, the three phases meet along a common line of contact (Figure 1d). In addition, the spreading coefficients are also able to predict the resulting wetting behavior in ternary blends composed of one major phase and two minor phases.[3,5]

This general framework has been used to predict the resulting morphology of multiphase polymer blends prepared by melt processing, and several papers have been published over the last 20 years concerning complex morphology development in ternary polymer blends.[6−19] Hobbs et al.[6] successfully used the spreading coefficients to predict encapsulation behavior in ternary and quaternary polymer blends of polystyrene, polycarbonate, poly(butylene terephthalate), poly(methyl methacrylate) and styrene−acrylonitrile copolymers. Guo et al.[8] used a variation incorporating interfacial area to predict the morphology

* Corresponding author. E-mail: basil.favis@polymtl.ca. Telephone: +1 514 340-4711 ext. 4527. Fax: +1 514 340-4159.

10.1021/ma802544q CCC: $40.75 © 2009 American Chemical Society
Published on Web 04/16/2009

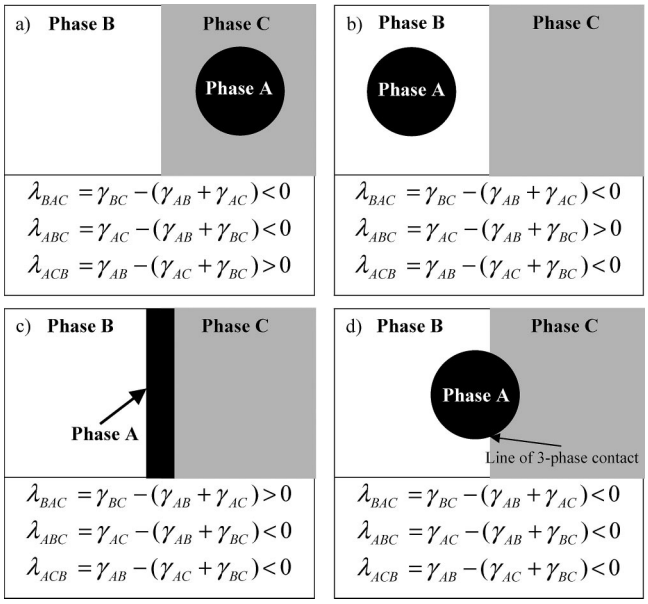

Figure 1. Possible morphologies in a ternary system composed of two major phases B and C (in white and gray) and one minor phase A (black), as predicted by the spreading coefficients. From part a to part c, morphologies displaying complete wetting, in which phases C, B and A respectively wet the AB, AC and BC interfaces. The morphology in part d displays partial wetting, in which none of the phases locates between the other two, resulting in a line of contact along which the three phases meet.

of droplet-in-droplet multicomponent blends of PS, PE, PP, and PMMA, but made no mention of the case of partial wetting. In a recent series of papers, Reignier et al.[11−14] conducted a detailed fundamental study on ternary HDPE/PS/PMMA blends with PMMA/PS core/shell composite droplets dispersed in an HDPE matrix. They showed that compositional, thermodynamic and viscoelastic properties of the materials all have significant effects on the morphology and the rheological properties of these blends. It is important to note that some important misconceptions still remain in the polymer blend literature concerning the use of the spreading coefficients. One often encountered is the prediction of the morphology in ternary polymer blends based on the calculation of only 1 or 2 spreading coefficients. This can lead to erroneous conclusions, especially when these are negative. In ternary blends, three spreading coefficients are necessary to correctly predict the resulting morphology.

Discrepancies have in some cases been observed between spreading coefficient predictions and experimental results. Among the causes, it has been shown that kinetic effects related to the viscosity and elasticity of the materials can sometimes have significant impacts when polymer blends are prepared by melt processing.[7,12] This is especially the case when kinetic contributions, such as phase viscosity, are relatively high. For example, Reignier et al.,[12] using Van Oene's concept of a dynamic interfacial tension,[20] showed a reversal of the PMMA/PS core/shell composite droplet morphology in a HDPE/PS/PMMA ternary blend due to elastic effects, even though the PMMA/PS core/shell structure is predicted by spreading coefficients and is usually observed experimentally in a HDPE matrix.[8,11−14] However, it is clear that the minimization of the interfacial free energy is a major driving force in the morphology development of multicomponent blends prepared by melt mixing.

Most of the work published so far on ternary polymer blends has studied morphology formation related to complete wetting, while partial wetting is rarely mentioned.[17−19] Horiuchi et al.[19] observed partial encapsulation in ternary blends of polyamide-6/polycarbonate/polystyrene (PA6/PC/PS) and polyamide-6/polycarbonate/styrene−(ethylene−butylene)−styrene triblock copolymer (PA6/PC/SEBS). They were able to switch to complete encapsulation by using reactive species of PS and SEBS grafted with maleic anhydride (PS-*g*-MA and SEBS-*g*-MA). In addition, a few papers have used the Neumann triangle method to measure interfacial tensions between different polymer pairs.[21−23] In that method, a droplet of polymer A is placed between two films of polymer B and C. After melting, the droplet of polymer A reaches an equilibrium geometry, and the three phases meet along a common line of contact. For this method to be applicable, the three spreading coefficients must be negative, which corresponds to partial wetting, as illustrated in Figure 1d. The relative magnitude of the interfacial tensions can then be obtained by measuring the contact angles between the phases. Hyun et al.,[21] Kim et al.,[22] and Zhang et al.[23] have used this method to measure interfacial tensions for ternary combinations of polypropylene/polystyrene/poly(methyl methacrylate) (PP/PS/PMMA) and polystyrene/poly(butylene terephthalate)/poly(methyl methacrylate) (PS/PBT/PMMA) with and without the addition of a small amount of poly(styrene-*co*-glycidyl methacrylate) (PS-GMA). For this last case, the PS-GMA reacted with the PBT to form a PBT-graft-PS copolymer, lowering the PS/PBT interfacial tension. This modification significantly affected the geometry of contact between the phases, confirming the sensitivity of the Neumann triangle method to measure variations of the interfacial tensions.

The objective of this paper is to report on a novel partial-wetting type of microstructure formation resulting in the close-packing of PS droplets at an HDPE/PP interface during melt processing. The relative position of the PS droplets at the interface and their preferred interaction with the other blend components will be studied and interpreted via an analysis of interfacial tension and interfacial saturation effects. Finally, the special case of coalescence of the PS droplets at the HDPE/PP interface will be examined by studying the influence of quiescent annealing time and selective interfacial modification with an SEB diblock copolymer.

Table 1. Materials Characteristics

polymers	$M_n \times 10^{-3}$ (g/mol)[a]	melt index (g/10 min)[a]	$\eta^* \times 10^{-3}$ (Pa·s)[b] at 200 °C and 25 s^{-1}	$\eta_0 \times 10^{-3}$ (Pa·s)[c] at 200 °C
HDPE		8	0.42	1.1
PP	89	35	0.27	0.71
PS	95 (M_w)	14	0.49	4.04
SEB	67			

[a] Obtained from suppliers. [b] Modulus of the complex viscosity at a frequency of 25 s^{-1}. [c] Zero-shear viscosity.

2. Experimental Methods

2.1. Materials. Three homopolymers and one diblock copolymer were used. A barefoot resin of high-density polyethylene, HDPE 3000, was supplied by Petromont. Polypropylene PP PD702 was obtained from Basell and polystyrene PS 615APR from the Dow Chemical Company. SEB CAP4741, a commercial 1,4-hydrogenated styrene−(ethylene−butylene) diblock copolymer with 30% styrene and 70% ethylene−butylene, was supplied by Shell. The materials characteristics are listed in Table 1.

2.2. Rheology. Rheological characterization of the homopolymers was performed in dynamic mode using a SR-5000 constant stress rheometer from TA Rheometrics. The experiments were performed using oscillatory measurements in a parallel plate geometry with a gap of 1.0 mm under a nitrogen atmosphere. The stability of the materials was controlled at 1 Hz and 200 °C. Stress sweeps at 0.1 and 10 Hz were performed to identify the region of linear viscoelasticity. Frequency sweeps were subsequently performed to obtain the zero-shear viscosity of the pure homopolymers, which has been extrapolated by using the modulus of the complex viscosity at low frequencies when the plateau value was reached, the loss

Table 2. Interfacial Tensions by the Breaking Thread Technique and Spreading Coefficients

polymer pairs	interfacial tensions γ (mN/m)	spreading coefficients λ (mN/m)	
HDPE/PS	4.9 ± 0.6	$\lambda_{HDPE/PS/PP}$	-6.5 ± 1.3
PP/PS	3.5 ± 0.2	$\lambda_{HDPE/PP/PS}$	-0.5 ± 1.3
HDPE/PP	1.9 ± 0.5	$\lambda_{PP/HDPE/PS}$	-3.3 ± 1.3

angle being sufficiently near 90° to consider the homopolymers as nonelastic Newtonian fluids. The rheological properties are reported in Table 1.

2.3. Interfacial Tension Measurement. All interfacial tensions were measured using the breaking thread method.[24,25] For the $\gamma_{HDPE/PS}$ and $\gamma_{PP/PS}$ interfacial tensions measurements, PS threads with diameters ranging from 30−60 μm were first annealed at 100 °C for 24 h under vacuum to remove the residual stress. PS threads were subsequently sandwiched between HDPE and PP films respectively. For the $\gamma_{HDPE/PP}$ interfacial tension measurement, PP threads were sandwiched between HDPE films. Measurements were then performed at 200 °C using an Optiphot-2 microscope from Nikon and a Mettler FP-82HT hot-stage connected to a Mettler FP-90 central processor. Digital images were captured and analyzed using Streampix v.III and Visilog v.6.3 software applications, provided by Norpix. Between five and ten measurements were obtained for each reported interfacial tension value, except for the $\gamma_{HDPE/PP}$ tension for which only two were considered. The results are reported in Table 2. As a matter of comparison, Guo et al.[8] reported values of 5.9, 5.1, and 1.1 mN/m respectively for the HDPE/PS, PP/PS and HDPE/PP interfacial tensions, which follow similar trends to ours. The results we obtained are typically comparable with those from other publications.[8−10,14,15,26]

2.4. Blend Preparation and Annealing. HDPE/PP/PS blends with constant volume compositions of 45/45/10 with either 0%, 1%, or 15% SEB (based on the volume of PS) were prepared in a Plasti-Corder Digi-System internal mixer from C.W. Brabender Instruments Inc. at 200 °C and 50 RPM for 8 min under a constant nitrogen flow. A small amount (0.2% by weight) of Irganox B-225 from Ciba-Geigy was added to the blends in order to prevent thermal degradation. In order to uniformly distribute and maximize the migration of the SEB to the HDPE/PS interface, pure PS was initially blended with 1% or 15% SEB based on the PS volume content at 180 °C and 50 RPM for 5 min under a constant nitrogen flow. The ternary blends were prepared subsequently with the required amount of PS+SEB. After blending, the blends were quenched in cold water to freeze-in the morphology. Blends were annealed at 200 °C for 0, 15, 30, 60, and 120 min respectively. They were plunged into cold water to freeze-in the morphology.

2.5. Scanning Electron Microscope Observations. Samples were cryogenically microtomed using a Leica RM2165 microtome equipped with an LN21 cooling system. For SEM observations, the PS phase was then extracted at room temperature for three days using cyclohexane as a selective solvent and dried for 2 days at 60 °C under vacuum in an oven. The samples were then coated with a gold/palladium layer by plasma sputtering. SEM observations were conducted using a JEOL JSM 840 scanning electron microscope operated at 10 keV and 6×10^{-11} A.

2.6. Focused Ion Beam Sample Preparation and Atomic Force Microscopy Analysis. Samples for focused ion beam (FIB) preparation were first cryogenically microtomed. A gold-paladium layer was then deposited on the samples by plasma sputtering and, finally, the surface of the specimens was further smoothed by a focused ion beam treatment. Surface etching was performed using a Hitachi 2000A FIB with a Ga^+ focused ion beam operated at 30 keV and 3 nA, with an etching window of 120×10 μm^2 and a dwelling time of 3 μs. The etched surface was then analyzed by AFM in tapping mode using a Dimension 3100 scanning probe microscope from Veeco Instruments equipped with a Nanoscope IVa control module. The tips used were model PPP-NCH-W from Nanosensors, with a resonance frequency of 204−497 kHz, a force constant of 10−130 N/m, length and width of 125 ± 10 μm and 30 ± 7.5 μm, tip height of 10−15 μm, and radius <10 nm. Images were subsequently treated with the AFM software to remove the effects caused by the inclination of the samples and the curtain effect produced by FIB surface preparation. Details concerning the procedure are given in a previous paper.[27]

2.7. Image Analysis and Average Diameter Measurements. SEM micrographs were used to measure the average diameters in number and volume (d_n and d_v) of the PS droplets. The PS droplets to be analyzed were initially separated into two categories: (1) the PS droplets located at the HDPE/PP interface and (2) the PS droplets completely located inside the PP phase. The values of d_n and d_v were calculated for each of these two categories. The PS droplets on the micrographs were manually digitized using a digitizing table from Wacom and SigmaScan v.5 software. Since microtomy does not generally cut the PS particles at the equator, and to account for polydispersity effects, the Saltikov correction procedure[28] was also applied in order to obtain corrected values of the diameters. Between 100 and 500 PS droplets were used to perform the calculations when possible, and the associated errors on the average diameter values go from 50% for the smallest average diameter values to 15% for the highest values.

3. Results and Discussion

3.1. State of the Morphology Right after Melt Processing. Immediately after melt processing, the microstructure of the 45/45/10 HDPE/PP/PS ternary blend without copolymer consists of small PS droplets ($d_n = 0.8$ μm) distributed in a cocontinuous HDPE/PP blend, as shown in Figure 2a. By selectively extracting the PS droplets with cyclohexane, it is possible to clearly distinguish the three phases. The voids correspond to the extracted PS droplets. The HDPE corresponds to the regions displaying a certain roughness and is a result of the crystalline structure of the HDPE. Finally, the PP phase corresponds to the smooth surface domains.

Since the spreading coefficients are all negative (Table 2), the predicted morphology corresponds to PS droplets located at the HDPE/PP interface, with a preference for the PP side, since the PP/PS interfacial tension is lower than the HDPE/PS one (Table 2). Experimentally, it should be noted that no PS particles are observed in the HDPE phase. However, only a portion of the PS droplets seem to be located at the HDPE/PP interface, with a definite tendency to locate on the PP side. Another fraction is located inside the PP phase. The segregation of the PS droplets at the HDPE/PP interface is thus incomplete and the theoretical prediction based on spreading coefficients is only partially observed. Note that we obtained similar results by using a PS with a much lower viscosity and also with a PP with a higher viscosity. The explanation might be related to the spreading coefficients values themselves. If we examine these more closely, it is relevant to note that $\lambda_{HDPE/PP/PS} = -0.5 \pm 1.3$ mN/m, a borderline value for partial wetting. In such a case, viscoelastic forces acting on the PS droplets during the mixing step are possibly strong enough to drive them from the HDPE/PP interface into the PP phase, even if the thermodynamic tendency indicates that the PS droplets are more stable at the HDPE/PP interface.[7,12,19]

If 1% of the SEB diblock copolymer is added to the blend (based on the PS content), very little effect on the PS phase size is observed, but it now appears that most of the PS droplets are located at the HDPE/PP interface (Figure 2b).

After adding 15% of the SEB copolymer to the blend, the morphology after melt processing shows significant differences (Figure 2c). The size of the PS droplets is much smaller ($d_n = 0.45$ μm) and they are now located inside the HDPE phase or at the HDPE/PP interface, with a preference for the HDPE side. In this case the PS droplets are excluded from the PP phase.

To further enhance the details of the morphology and the effect of the copolymer on microstructure formation, quiescent

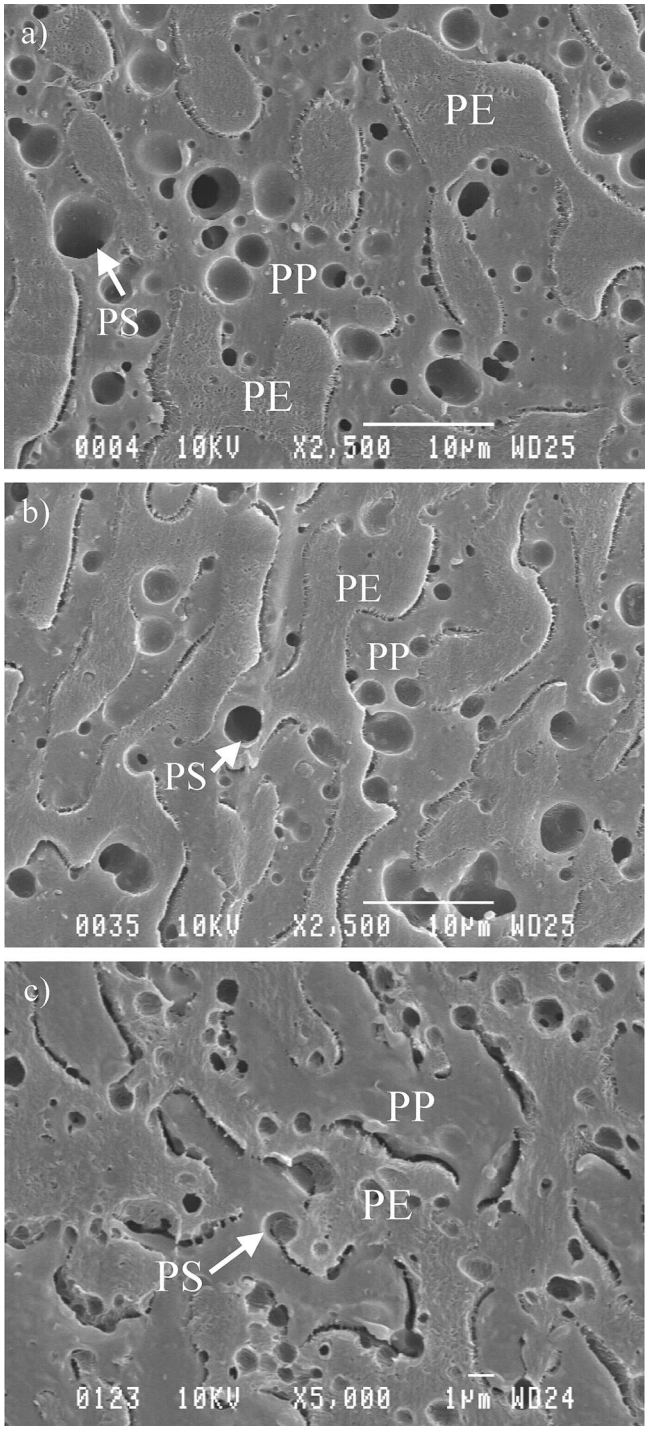

Figure 2. SEM micrographs of morphology of HDPE/PP/PS 45/45/10 vol % blends immediately after melt processing with (a) 0% SEB modifier, (b) 1% SEB, and (c) 15% modifier. Note that the PS phase has been selectively extracted using cyclohexane.

annealing of the blends was performed. It leads to spectacular differences in morphology development, as we will show in the next sections.

3.2. Evolution of the Morphology As a Function of Quiescent Annealing Time. *3.2.1. From Partial to Complete Segregation of the PS Droplets at the HDPE/PP Interface with the Addition of the SEB Copolymer.* Quiescent annealing of the uncompatibilized and compatibilized blends was performed for 15, 30, 60, and 120 min at 200 °C. In uncompatibilized blends, we observe a clear tendency for the PS droplets to locate at the HDPE/PP interface after quiescent annealing, in accordance with spreading coefficient predictions, although the segregation is incomplete and a significant number of PS particles still remain in the PP phase (Figure 3). Note, however, that the PS droplets are completely segregated from the HDPE phase. Also, the PS droplets located at the HDPE/PP interface clearly prefer the PP side, as shown in the focused ion beam/atomic force microscope (FIB−AFM) image of Figure 4, which is expected since $\gamma_{PP/PS} < \gamma_{HDPE/PS}$.

Furthermore, along the line of three-phase contact, the three contact angles θ_{PS}, θ_{HDPE}, and θ_{PP} (Figure 4) between the phases are very similar from one droplet to another. This strongly supports the case of partial wetting of the HDPE/PP interface by PS droplets, since constant contact angles are expected in that situation. This is a consequence of the equilibrium between the three interfacial tensions along the line of contact. As mentioned in the introduction, the Neumann triangle method can be used to measure the interfacial tensions between such materials in ternary immiscible blends displaying partial wetting.[3,21−23,29] It could also be interesting to study the effect of polydispersity on the formation of these systems. As demonstrated by Chaffin et al.,[30,31] oligomers and low molecular weight polymer chains tend to migrate to the interfaces, inducing a decrease of the interfacial tensions.[32,33] This could be measured by the modification of the 3-phase line of contact, if significant enough.

A spectacular transition occurs when the blend containing 1% SEB is annealed. The micrographs of Figures 5 and 6 show that almost all of the PS droplets are perfectly segregated at the HDPE/PP interface. No PS droplets whatsoever are observed in either the HDPE or PP phase. The difference is striking compared to the 0% SEB case of Figure 3. After 15 min of quiescent annealing, all the PS droplets are already located at the HDPE/PP interface and after 30 min, the structure is quite compact and the droplets appear to be squeezed together. Furthermore, comparing Figure 5d to Figure 3d, we can see that the PS droplets after 120 min are generally smaller in size compared to the 0% SEB case and that the HDPE and PP domains coarsen less rapidly. In Figure 7 an SEM micrograph is used to show the contour of an interface (as opposed to the single plane views shown in Figures 5 and 6) and a very dense array of PS droplets is clearly shown. To our knowledge, this is the first time that polymer droplets have been reported to perfectly self-organize at a polymer/polymer interface.

Furthermore, after 60 min of annealing time, the FIB/AFM image of Figure 8 shows that a significant fraction of the PS droplets have clearly relocated from the PP side of the interface at 0% SEB to the HDPE side of the interface when 1% SEB is added, supporting the notion that the SEB preferentially locates at the HDPE/PS interface and lowers the corresponding interfacial tension.

When 15% of SEB is added to the blend, almost all of the PS droplets are located either in the HDPE phase or at the HDPE/PP interface for all annealing times (Figures 9 and 10).

Hence, at 0% SEB modifier, we observe PS droplets located either at the HDPE/PP interface or in the PP phase. The addition of 1% SEB results in the exclusive location of the PS droplets at the HDPE/PP interface (a complete segregation of the PS droplets from both phases). At 15% SEB, the PS droplets are located either at the HDPE/PP interface or in the HDPE phase and are completely segregated from the PP phase. Note that the apparent debonding between the HDPE and PP phases in Figure 9 is probably due to the fact that the PS droplets are very small and form an almost complete layer at the interface, making it look like cracks between the phases when the droplets are selectively extracted. These results point toward an approach which can selectively control the location of dispersed particles

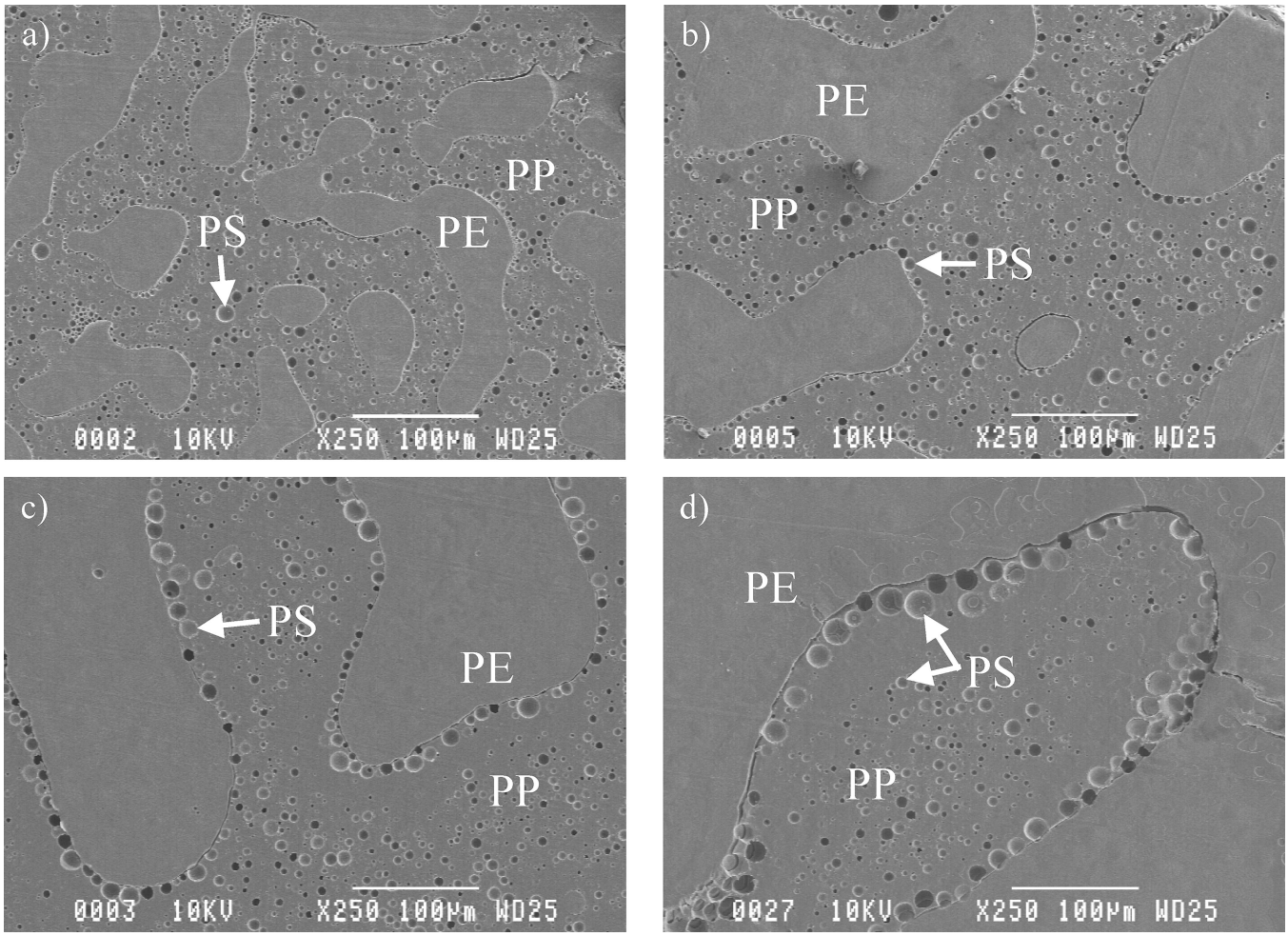

Figure 3. SEM micrographs of the ternary HDPE/PP/PS 45/45/10 vol % blend, 0% SEB, after (a) 15 min of annealing time at 200 °C, (b) 30 min, (c) 60 min, and (d) 120 min. Note that the PS phase has been extracted in order to facilitate the identification of the phases.

in a blend, either at an interface or in the volume of a particular phase.

3.2.2. Spreading Coefficient Mechanism. These morphology transitions can be predicted by the spreading coefficients if we suppose that the PS droplets and the copolymer distribution are in quasi-equilibrium after quiescent annealing. When no compatibilizer is added, the three spreading coefficients have the following values:

$$\lambda_{HDPE/PS/PP} = \gamma_{HDPE/PP} - (\gamma_{HDPE/PS} + \gamma_{PP/PS}) = 1.9 - (4.9 + 3.5) = -6.5 \text{ mN/m} \quad (2a)$$

$$\lambda_{HDPE/PP/PS} = \gamma_{HDPE/PS} - (\gamma_{HDPE/PP} + \gamma_{PP/PS}) = 4.9 - (3.5 + 1.9) = -0.5 \text{ mN/m} \quad (2b)$$

$$\lambda_{PP/HDPE/PS} = \gamma_{PP/PS} - (\gamma_{HDPE/PP} + \gamma_{HDPE/PS}) = 3.5 - (4.9 + 1.9) = -3.3 \text{ mN/m} \quad (2c)$$

The three negative values above predict partial wetting but with a preference for PP to encapsulate PS more than HDPE (Figure 11a).

To pull the droplets toward the HDPE phase, $\gamma_{HDPE/PS}$ must decrease. If $\gamma_{HDPE/PS}$ decreases by adding SEB, a first significant morphological transition is expected when $\gamma_{HDPE/PS} = 3.5$ mN/m. At that point, $\lambda_{HDPE/PS/PP}$ and $\lambda_{PP/HDPE/PS}$ become equal and are still negative, while $\lambda_{HDPE/PS/PP}$ remains negative. This implies that the driving forces for encapsulation of PP about PS and HDPE about PS are equivalent. As a result, partial wetting is

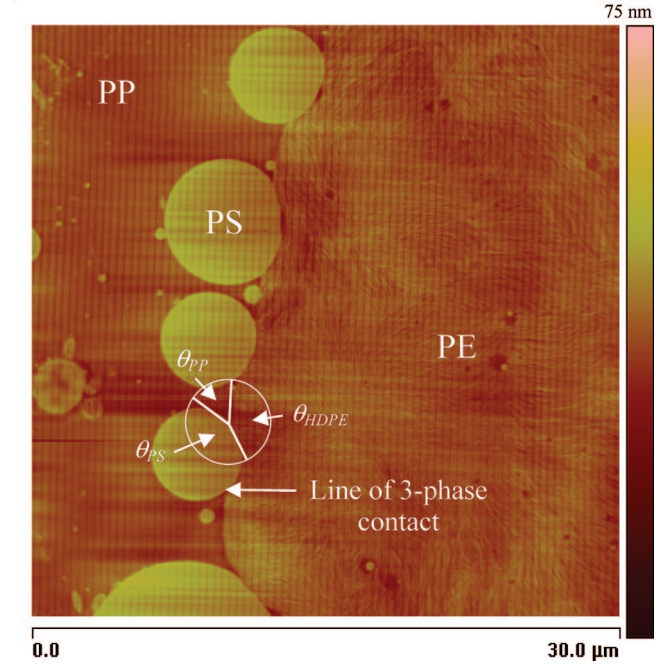

Figure 4. FIB−AFM image of the HDPE/PP/PS 45/45/10 vol % blend without compatibilizer, after 60 min of quiescent annealing time at 200 °C. Note that the contact angles θ_{HDPE}, θ_{PP}, and θ_{PS} are similar from one droplet to another, and the crystalline structure of the HDPE is clearly visible after FIB treatment.

still predicted, but with PS droplets symmetrically located at the HDPE/PP interface, with half of the PS droplet volume in the PP phase and the other half in the HDPE phase (Figure 11b).

If $\gamma_{HDPE/PS}$ decreases even further by increasing the concentration of the modifier at the HDPE/PS interface, the PS droplets will relocate on the HDPE side of the HDPE/PP interface (Figure 11c). A second significant morphological transition is expected when $\gamma_{HDPE/PS} \leq 1.6$ mN/m. At this point, $\lambda_{PP/HDPE/PS} \geq 0$ while the other two spreading coefficients remain negative. The system passes from partial to complete wetting, with the PS droplets located exclusively in the HDPE phase (Figure 11d). This sequence of morphological transitions corresponds to the one observed experimentally for the PS droplets in the present study, which confirms the affinity of the SEB for the HDPE/PS interface.

For the blend containing 1% SEB and annealed for 60 min, it clearly appears from the micrograph of Figure 6 and the FIB−AFM image of Figure 8 that the PS droplets are located on the HDPE side of the HDPE/PP interface. From this observation, and based on the discussion above, the modified HDPE/PS interfacial tension for that case is somewhere between 3.5 and 1.6 mN/m. Note that the measured interfacial tension for the unmodified HDPE/PS pair is 4.9 mN/m (see Table 2).

Similar conclusions are reached for the HDPE/PP/PS 45/45/10 blend containing 15% of SEB. Some of the PS droplets are on the HDPE side of the HDPE/PP interface, and some are completely in the HDPE phase. As a result, the HDPE/PS interfacial tension after modification with 15% SEB is probably close to 1.6 mN/m to account for the significant number of PS droplets within the HDPE phase.

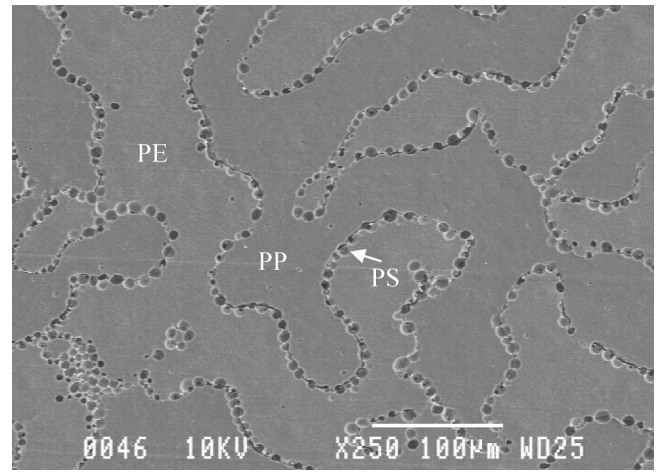

Figure 6. SEM micrograph of the HDPE/PP/PS 45/45/10 vol % blend with 1% SEB (based on the PS content) annealed for 60 min at 200 °C. The PS droplets are almost all segregated at the HDPE/PP interface, preferentially on the HDPE side, and form a closely packed array. Note that the PS phase has been extracted in order to facilitate the identification of the phases.

It appears clear that the morphological transitions observed when SEB is added to the ternary blend are the consequences

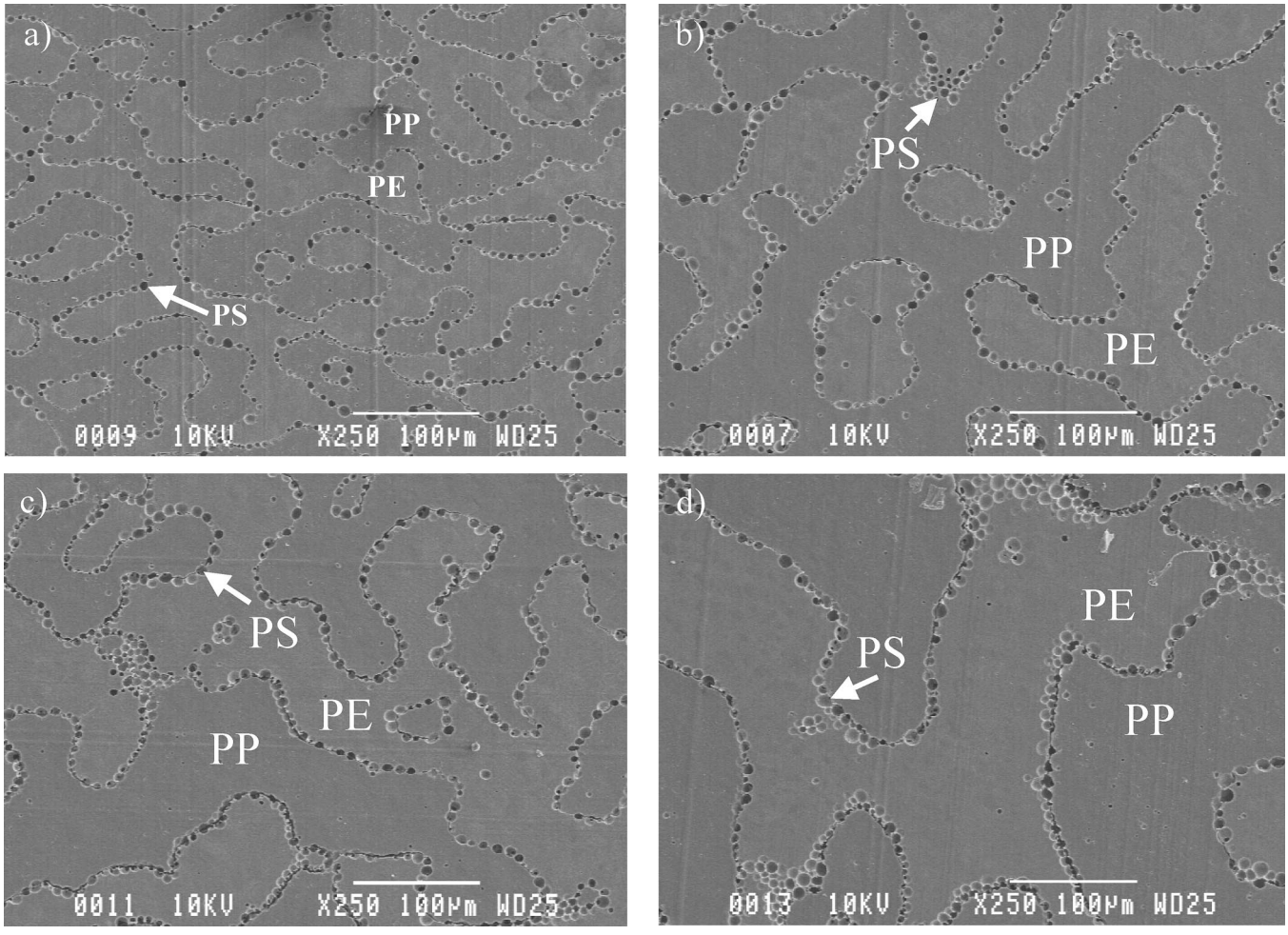

Figure 5. SEM micrographs of the ternary HDPE/PP/PS 45/45/10 vol % blend with 1% SEB based on the PS content after (a) 15 min of annealing time at 200 °C, (b) 30 min, (c) 60 min, and (d) 120 min. Note that the PS phase has been extracted to facilitate the identification of the phases.

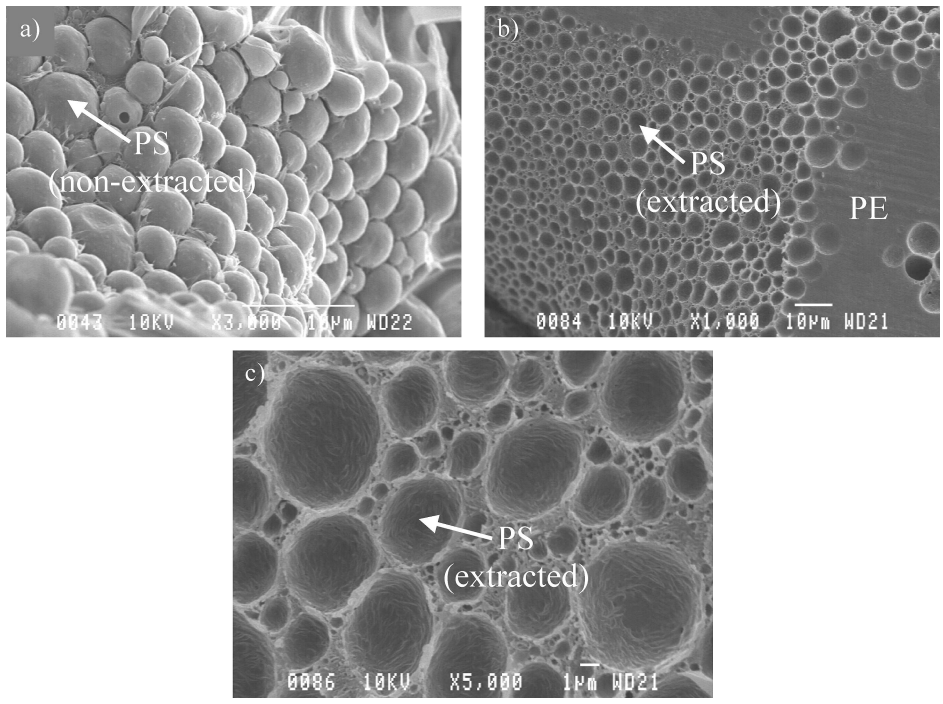

Figure 7. SEM micrographs showing the PS droplets closely packed at the HDPE/PP interface after 120 min of quiescent annealing time. (a) View of the nonextracted PS droplets at the HDPE interface in blends containing 1% SEB, when the PP phase is pulled away from the interface by cryofracture. Note the deformation of some PS droplets when they are touching each other. (b) View of the HDPE/PP interface in blend containing 1% SEB modifier, after removal of PP by cryofracture and selective extraction of the PS droplets with cyclohexane. (c) Close-up view of micrograph b.

of (1) the preference of the copolymer to locate at the HDPE/PS interface and (2) the resulting decrease of $\gamma_{HDPE/PS}$.

3.2.3. Variation of the HDPE/PS Interfacial Tension As a Function of the Areal Density in Copolymer. For the compatibilized PS droplets, it is possible to calculate an apparent areal density in copolymer at the HDPE/PS interface. To do so, we must make the assumption that all the SEB migrates to the HDPE/PS interface during melt processing and subsequent quiescent annnealing. The apparent areal density Σ of the copolymer located at the HDPE/PS interface is calculated by dividing the amount of copolymer in the PS droplet, equal to $4\pi\, r_{HDPE/PS}{}^3\varphi_{copo}N_{AV}/3M_{copo}$, by the area of the HDPE/PS interface, which is equal to $2\pi\, r_{HDPE/PS}{}^2\,(1 - \cos\phi_{HDPE/PS})$:[34−37]

$$\Sigma = \frac{2r_{HDPE/PS}\phi_{copo}N_{AV}}{3M_{copo}(1 - \cos\varphi_{HDPE/PS})} \tag{3}$$

$r_{HDPE/PS}$ is the radius of curvature of the HDPE/PS interface defined in Figure 12 (here equal to 4.8 μm, the radius of the PS droplet); φ_{copo} is the SEB copolymer concentration in the blend in g/100 mL of PS (here 1 g SEB/100 mL of PS); N_{AV} is Avogadro's number; M_{copo} is the copolymer molecular weight, and $\phi_{HDPE/PS}$ is the angle defined and illustrated in Figure 12 (which we approximate at 135°).

The calculated apparent areal density Σ is approximately 0.17 SEB molecules per nm^2, or 6 nm^2 per copolymer molecule, a value close to previously estimated saturation values.[34−39] As a matter of comparison, Polizu et al.[38] reported an almost identical apparent areal density value at saturation of 0.18 molecules/nm^2 in a PS/EPR blend compatibilized with an SEB diblock copolymer similar in composition and molecular weight to the one we used. Cigana et al.[34,35] reported a similar areal density value at saturation of 0.18 molecules/nm^2 for compatibilized PS/EPR blends with a similar diblock copolymer, while Li et al.[39] reported similar trends in HDPE/PS blends compatibilized with SEB and SEBS diblock and triblock copolymers. Macosko et al.[36] reported a saturation value of 0.12 molecules/nm^2 for a deuterated PS-*block*-PMMA of M_n = 100 900. Using a scaling law, they estimated the saturation value at 0.145 molecules/nm^2 for a similar diblock of M_n = 55 000. Adedeji et al.[37] reported apparent areal densities between 0.1 and 0.2 molecules/nm^2 for diblock PS-*b*-PMMA copolymers in binary blends of poly(cyclohexyl methacrylate) and poly(methyl methacrylate), near theoretical saturation values.

Consequently, one can estimate that the HDPE/PS interfacial tension modified with 1% of SEB copolymer is somewhere between 3.5 and 1.6 mN/m, for a surface coverage of about 6 nm^2/copolymer molecule or an areal density of 0.17 molecules/nm^2. This is an important result, since it is still a challenge to obtain quantitative data relating the variation of the interfacial tension as a function of the areal density of copolymer in a blend prepared by melt processing.

3.2.4. Comparison of Interfacial Coalescence to Bulk Coalescence. In order to examine coalescence phenomena of the PS droplets, the particle size was quantified as a function of the quiescent annealing time. The PS droplets were divided into two categories: (1) the PS droplets located at the HDPE/PP interface and (2) the PS droplets located in the PP bulk phase. The number and volume average diameters, d_n and d_v, were measured for each PS droplet category as a function of annealing time, for both uncompatibilized and compatibilized blends. Since initially, before annealing, it is difficult to distinguish which particles are at the interface and which are in the PP phase, the average diameter right after melt mixing is used for all the PS droplets. As a reference, we also give the average diameter of the PS droplets as a function of annealing time for the 80/20 PP/PS binary blend. Note that both the d_n and d_v results follow similar trends, so only the results for d_n are reported here.

After annealing for 30 min, the PS droplets located at the HDPE/PP interface in the uncompatibilized blend increase from

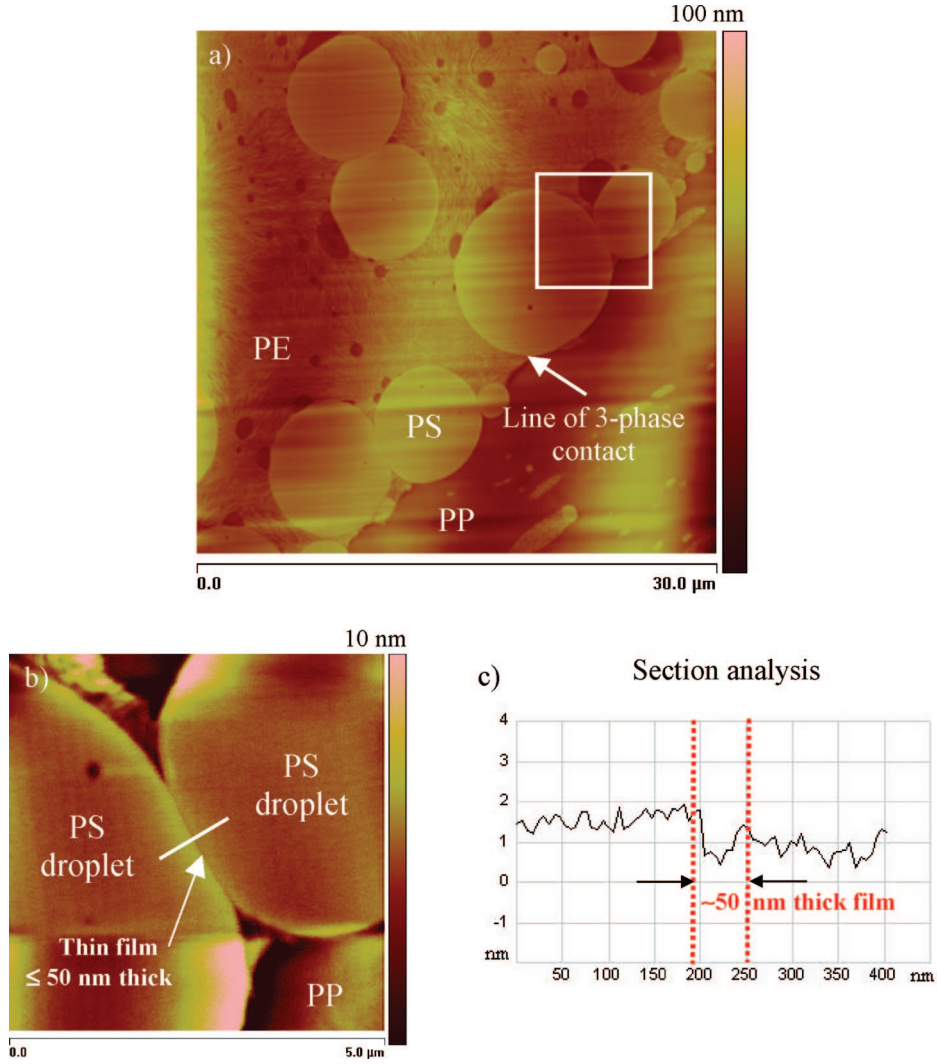

Figure 8. (a) FIB−AFM image of the 45/45/10 HDPE/PP/PS blend containing 1% SEB after 60 min of quiescent annealing time, (b) close-up of the region delimited by the white square in part a, showing a very fine line between the two PS droplets and a visible deformation of the two droplets along the contact area, and (c) section analysis along the white line in part b, giving the thickness of the film separating the two PS droplets.

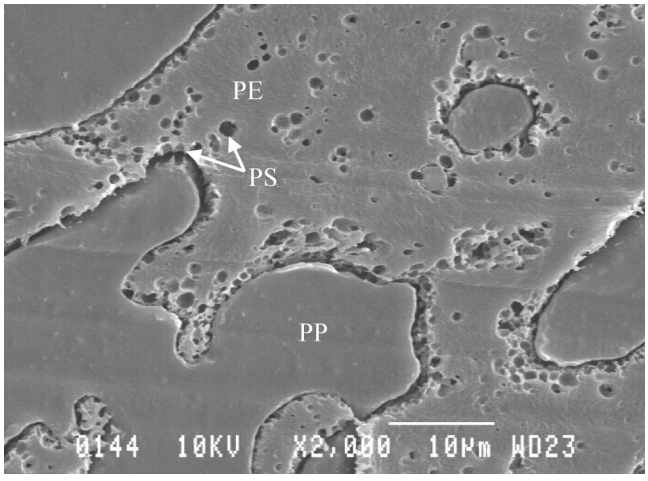

Figure 9. SEM micrograph of the ternary HDPE/PP/PS 45/45/10 vol % blend with 15% SEB (based on the PS content) after 60 min of quiescent annealing time. Note that the PS phase has been extracted in order to facilitate the identification of the phases.

an initial 0.8 μm to approximately 3.7 μm in diameter (Figure 13a). If the annealing time is prolonged to 60 and 120 min, a significant increase in average droplet size is observed for the PS droplets located at the HDPE/PP interface (with $d_n = 12.7$ μm after 120 min), while the PS droplets located in the PP phase remain nearly constant in size and are comparable to the PS droplets in the binary PP/PS blend (with $d_n = 1.5$ μm after 120 min of annealing time). Clearly, and not unexpectedly, PS particles confined to the interface via the interfacial driving force discussed above demonstrate significantly higher coalescence due to a greater probability of collision with neighboring droplets, especially since the HDPE/PP interfacial area decreases during the quiescent annealing procedure and brings the PS droplets closer to one another. The HDPE and PP networks coarsen during quiescent annealing and the available interfacial area for the PS droplets located at the HDPE/PP interface decreases.[40−44] This increases the rate of collisions and coalescence between the PS droplets located at the HDPE/PP interface compared to the ones located in the PP volume. Coalescence of the PS droplets located at the interface results in a decrease of the interfacial energy of the system. Although there is in an increase of the HDPE/PP interfacial area and energy after this process, the associated decrease of the HDPE/PS and PP/PS interfacial areas results in a negative overall interfacial energy variation, leading to a more stable state after coalescence.

For the 1% compatibilized blend, the number average diameter of the PS droplets prior to annealing is similar to the

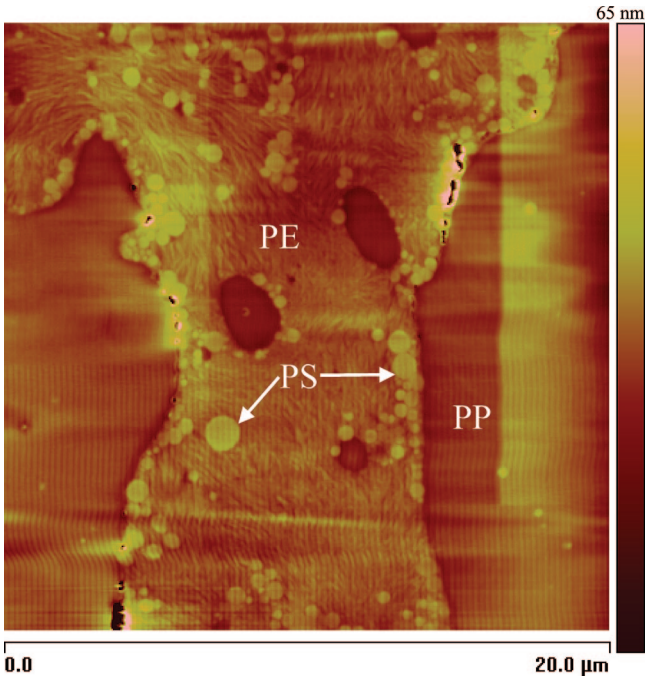

Figure 10. FIB−AFM image of the HDPE/PP/PS 45/45/10 blend containing 15% SEB after 60 min of quiescent annealing time at 200 °C. Almost all of the PS droplets are either at the HDPE/PP interface, forming clusters, or, in the HDPE phase, confirming the affinity of the copolymer for the HDPE/PS interface.

one without copolymer at 0.8 μm and reaches 7.5 μm after 120 min of quiescent annealing time for the PS droplets located at the interface (Figure 13b). This can be compared to 1.7 μm for the very few droplets located in the PP phase. Finally, for the 15% SEB compatibilized blend, the average droplet diameter does not change much with annealing time and stays at approximately 0.5 μm even after 120 min of annealing time for both the PS droplets at the HDPE/PP interface and in the HDPE (Figures 2c, 9 and 10). This demonstrates, for this latter case, an almost complete coalescence suppression both at the interface and in the bulk.

3.2.5. Effect of the SEB Copolymer on Interfacial Coalescence Rates. Clearly, significant differences are observed between the interfacial coalescence rates of the PS droplets depending on whether the blends contain either 0% or 1% SEB (Figure 14). First of all, the coarsening rate of the PS droplets containing 1% SEB at the HDPE/PP interface is initially more rapid as compared to the case without compatibilizer.

The average diameter increases from 0.8 to 4.3 μm in the case of 1% SEB after 15 min of annealing time, as compared to 0.8 to 1.9 μm in the case of 0% SEB for the same annealing time. However, after the first 15 min of quiescent annealing, the coalescence rate of the 1% SEB compatibilized PS droplets at the HDPE/PP interface significantly decreases and falls below the coalescence rate of the PS droplets without the SEB compatibilizer. This ultimately leads to a significantly smaller average diameter compared to the uncompatibilized case after 120 min of annealing time. Moreover, the coalescence rate of the compatibilized system is very slow (virtually zero) between 60 and 120 min, the average diameter increasing from only 6.3 to 7.5 μm, as compared to 6.5 to 12.7 μm for the uncompatibilized case.

When 1% of the SEB copolymer is added, the driving force for partial wetting increases, resulting in significantly more PS particles at the interface at low annealing times compared to the 0% case. This also results in a greater collision probability between neighboring PS droplets. Furthermore, at low annealing times, the PS droplets are preferentially located on the PP side of the interface (see Figures 2b and 5a), thus significantly reducing the interfacial area modified by the copolymer. This could explain why the coalescence rate is faster initially for the 1% SEB blend. At longer annealing times, the PS droplets clearly relocate on the HDPE side of the interface (see Figures 5, 6, and 8) with an areal density in SEB close to interfacial saturation values as discussed above. This results in significant steric hindrances between neighboring droplets and the suppression of coalescence of the PS droplets,[45,46] explaining the plateau effect observed in Figure 13b and 14 for long annealing times. Figures 6 and 7 also support an explanation based on steric repulsion as they show a very compact array of PS droplets after the addition of 1% SEB and at 60 min of annealing. In Figure 7c, it clearly appears that although the droplets are packed together, they remain separated by a thin layer. Also, we can see smaller droplets in the interstices between the larger ones. The FIB−AFM image of Figure 8 clearly shows PS droplets so close together that some deformation is observed, although what appears to be a very thin film separates them. The section analysis of Figures 8b and c show that this film is very thin (most probably below 50 nm, although we are close to the resolution limit of the apparatus). These features are not observed for the 0% SEB blend, and support the idea of coalescence suppression by steric hindrance. These fully emulsified droplets serve not only to reduce the coalescence of PS at the interface, but also to stabilize the cocontinuous HDPE/PP structure from further coarsening. This feature of interfacially modified PS droplets at the HDPE/PP interface is similar to the case of solid microparticles stabilizing Pickering emulsions[47−54] and bijels.[55,56]

Important questions will need to be addressed related to the initial distribution of the copolymer in the blend and its subsequent redistribution toward the HDPE/PS interface. These questions will be addressed in a future work.

3.2.6. Conceptual Mechanism for the Assembly of PS Droplets at the Interface. Since the coalescence rate of the binary PS in PP blend is low, one can readily conclude that the mobility of PS droplets in the PP phase during annealing is low. How then does one explain the perfection of the formation of the close-packed PS droplet structure at the interface arising from annealing? Two factors that can have a major impact on the formation of the close-packed structure are (1) the stability of the PS droplets at the HDPE/PP interface due to interfacial forces and (2) the mobility of the HDPE/PP interface. The first factor was discussed in the previous sections. The second factor, however, is also important. What appears to be occurring is a "sweeping" effect related to the movement of the HDPE/PP interface (Figure 15).

During annealing, the cocontinuous HDPE and PP domains coarsen rapidly, as can be seen in the micrographs of Figures 3 and 5. During this coarsening, the overall HDPE/PP interfacial area decreases, as demonstrated in earlier papers studying coarsening of cocontinuous binary blends.[40−44] This implies a movement of the HDPE/PP interface, which can grab PS droplets located in the PP phase while moving, increasing the number of PS droplets at the HDPE/PP interface. Since the PS droplets are more thermodynamically stable when located at the HDPE/PP interface, this sweeping effect acts like a net that grabs and holds onto the droplets. This "sweep and grab" effect is probably more important at the beginning of the coarsening process, since the HDPE/PP interfacial area is higher initially. Thus, a strategy to increase the amount of PS particles at the HDPE/PP interface could be to have a very fine HDPE/PP cocontinuous blend at the onset of the annealing process.

The coarsening of the HDPE and PP phases and the resulting decrease in interfacial area has another important impact. The PS droplets located at the interface draw closer to one another

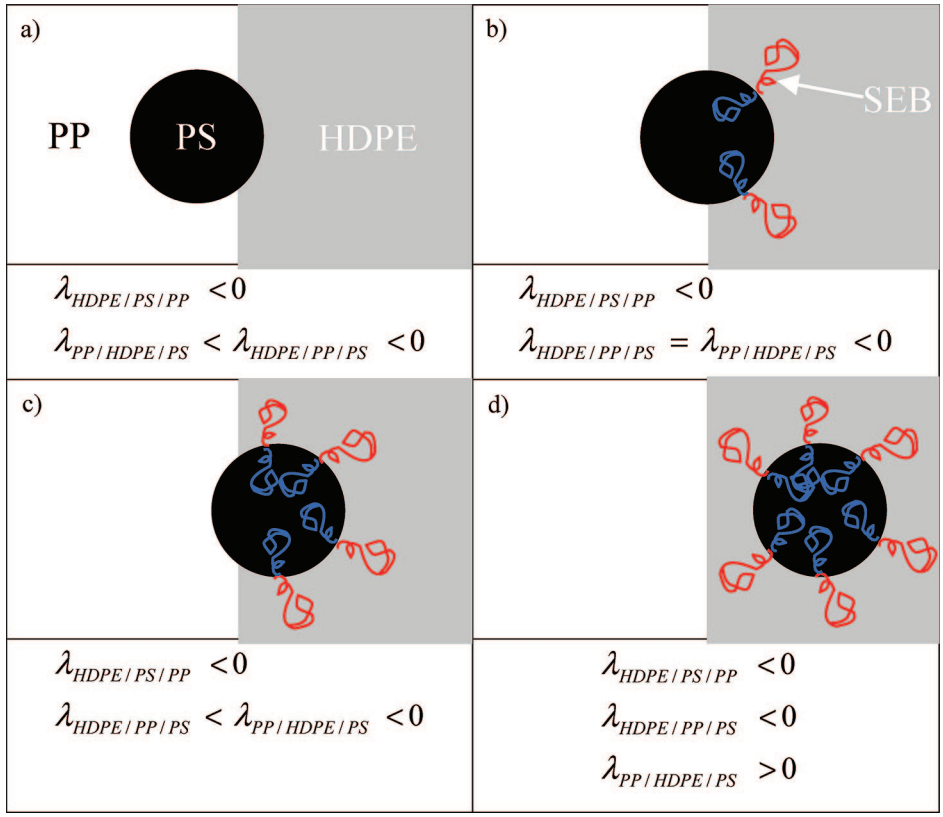

Figure 11. Effect of the SEB copolymer on morphology: (a) initial morphology, when no compatibilizer is added; (b) $\gamma_{HDPE/PS}$ modified with SEB is equal to $\gamma_{PP/PS}$ (3.5 mN/m), and PS is symmetric at the HDPE/PP interface; (c) 1.6 mN/m < $\gamma_{HDPE/PS}$ modified with SEB < 3.5 mN/m, PS droplets are on the HDPE side of the HDPE/PP interface and d) $\gamma_{HDPE/PS}$ modified with SEB < 1.6 mN/m, PS droplets are in HDPE.

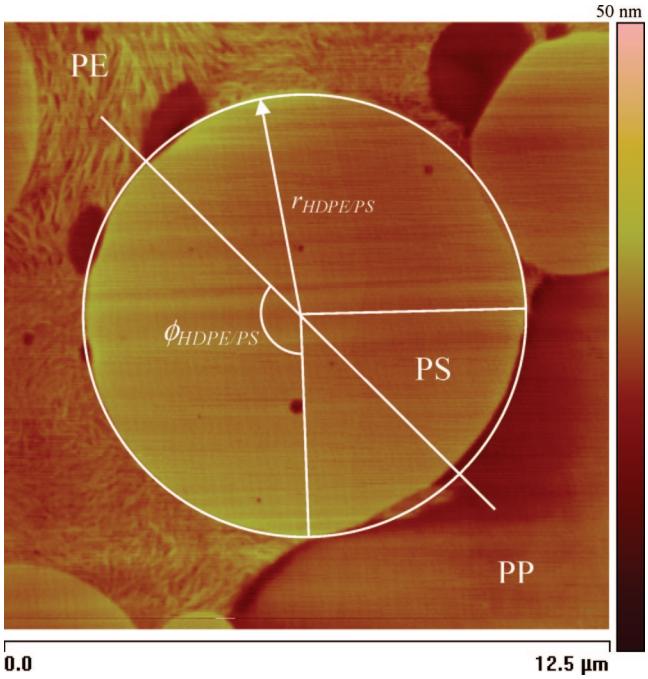

Figure 12. FIB−AFM image of the HDPE/PP/PS 45/45/10 vol % blend containing 1% SEB after 60 min of quiescent annealing time at 200 °C. The PS drop has clearly relocated toward the HDPE side of the HDPE/PP interface due to the copolymer.

and contact between the droplets becomes more frequent. As the interfacial area decreases significantly, the PS droplets end up forming a tightly packed structure, as shown in Figures 3, 5, and 7. Once closely packed at the interface, the time it takes for droplets to approach one another is very small, and the dynamics of coalescence becomes controlled by the time it takes to drain and rupture the film between adjacent PS droplets. This effect is particularly evident when the copolymer is added to the blend. In that case, the PS droplets do not coalesce fast enough and this actually, in turn, slows down the whole HDPE/PP coarsening process. This feature is particularly evident in Figures 3d and 5d where it can be seen that HDPE and PP domains are finer after 120 min of annealing time for the 1% SEB compatibilized blend compared to the 0% case. Thus, by controlling the coalescence rate of the PS droplets at the interface using a copolymer, it is also possible to control the coalescence rate of the cocontinuous HDPE and PP networks.

3.2.7. Similarities with Pickering Emulsions and Bijels. The morphology of HDPE/PP/PS blends is closely related to the structure formation of Pickering emulsions[47−54] and bijels.[55,56] Pickering emulsions are droplet-in-matrix binary fluid mixtures, while bijels are binary cocontinuous fluid systems. In both cases, their microstructure is stabilized against coalescence by a film of submicrometer-size particles at the interface that creates a kinetic barrier which slows down and ultimately inhibits coarsening. In this work, compatibilized PS droplets act in a similar way to prevent the coarsening of the continuous HDPE and PP phases.

In all these situations, the selective segregation of the particles to the interface seems to be of thermodynamic origin and results in a significant decrease of the interfacial free energy, similar to our HDPE/PP/PS blends. Binks and Lumsdon,[53] by selectively controlling the hydrophilic/hydrophobic character of their silica nanoparticles, were able to control wettability and, in turn, study the stability of their emulsions as a function of the surface properties of the particles. A similar study is underway with our HDPE/PP/PS blends, in which we will examine copolymer efficacy at stabilizing the structure of our ternary HDPE/PP/PS

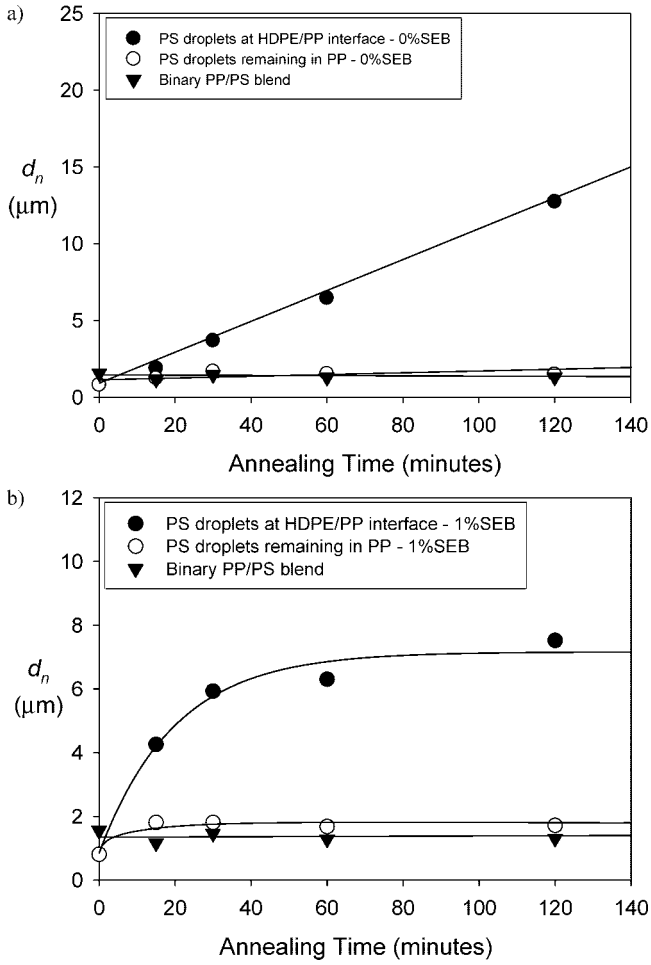

Figure 13. Number average diameter d_n of the PS droplets, at the interface, in the bulk, and for the binary PP/PS blend, as a function of annealing time: (a) 45/45/10 HDPE/PP/PS blend without SEB and (b) 45/45/10 HDPE/PP/PS blend with 1% SEB based on PS content.

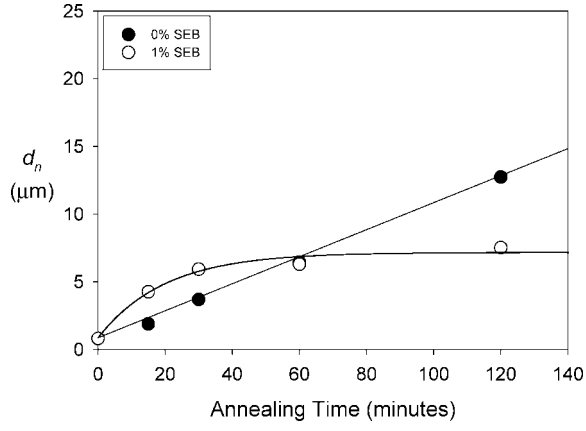

Figure 14. Comparison between the number average diameters in number d_n for PS droplets at the HDPE/PP interface with 0% and 1% SEB as a function of annealing time.

blends. Interestingly, thermodynamically stable Pickering emulsions have also been reported recently.[48]

In another line of work, segregation of carbon black and silica particles to the interface has also been investigated in binary polymer blends.[57−60] A stabilizing effect against coalescence was also reported, together with significant modifications of the rheological and morphological properties such as an extension of the dual-phase region over a broader composition range. Furthermore, an ultralow percolation threshold for the carbon

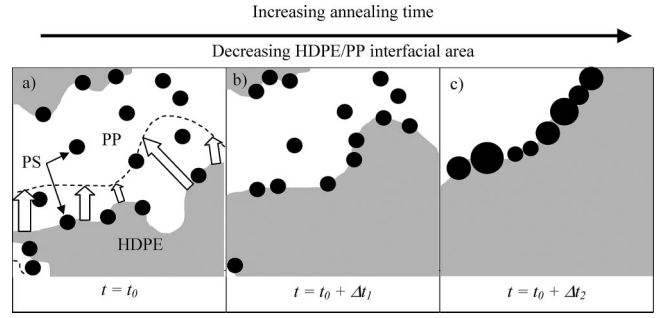

Figure 15. Schematic showing the formation of the PS droplets close-packed structure. The HDPE network is in gray, the PP network is white and the PS droplets are in black. During annealing, the HDPE and PP networks coarsen and the HDPE/PP interface moves (indicated by the arrows in part a). The resulting movement of the HDPE/PP interface results in PS droplets initially in the PP relocating at the HDPE/PP interface, in part b. At the same time, the droplet size increases by coalescence and the close-packed structure forms due to the decrease in HDPE/PP interfacial area (c).

black particles was obtained due to its selective localization at the interface in binary PE/PS and PMMA/PS blends,[59,60] resulting in a significant increase of the electrical conductivity.

Partial wetting can yield a number of novel polymer blend structures. A pertinent question we are now investigating is how many ternary systems display this property. We are also investigating the potential of the Neumann triangle method applied to these systems as an approach to obtain values of the interfacial tension both in the presence or absence of an interfacial modifier.

Clearly, the control of the wetting properties is a very promising approach to achieve novel complex morphological microstructures in multicomponent polymer blends.

4. Conclusion

This paper reports, for the first time, on the self-assembling of PS droplets into a close-packed array at the HDPE/PP interface in melt-processed HDPE/PP/PS ternary polymer blends. This highly organized microstructure is induced by the partial wetting of the HDPE/PP interface by the PS droplets. The close-packed droplet array at the interface is accentuated by quiescent annealing due to a "sweep and grab" effect induced by the coarsening of the HDPE/PP cocontinuous microstructure. The affinity of the PS droplets for the HDPE/PP interface can be predicted by spreading coefficient theory and can be further controlled by the addition of an SEB diblock copolymer. The addition of 1% SEB results in the almost complete localization of the PS droplets at the HDPE/PP interface. As the copolymer content increases, the PS droplets migrate from the PP phase and PP side of the HDPE/PP interface to the HDPE side and HDPE phase. This additional morphology transition can also be explained using the spreading coefficients and is a result of the particular affinity of the SEB copolymer for the HDPE/PS side of the interface. Using the spreading coefficients, it has been estimated that the copolymer reduces the HDPE/PS interfacial tension from 4.9 mN/m to about 1.6 mN/m for an apparent areal density of SEB of approximately 0.17 copolymer molecule/nm^2 at the HDPE/PS interface, a value close to reported saturation values. Below 1.6 mN/m the spreading coefficients predict complete wetting with PS droplets in the HDPE phase. An examination of the interfacial coalescence of these systems shows that the coalescence rate of the unmodified PS droplets located at the HDPE/PP interface is significantly higher than that for the PS droplets located in the PP bulk phase. The addition of 1% SEB copolymer results in an even higher coalescence rate for PS droplets at the interface, early in the quiescent annealing procedure. However, coalescence rapidly

decreases and falls to virtually zero after 60 min due to the saturation of the HDPE/PS interface by the SEB copolymer. It is shown that when interfacially modified PS droplets are located at the HDPE/PP interface they also serve to completely stabilize the cocontinuous HDPE/PP network from further coalescence.

This work opens exciting perspectives in generating novel complex microstructures in polymer blends.

Acknowledgment. The authors gratefully acknowledge the financial support received from the Natural Sciences and Engineering Research Council of Canada (NSERC). The authors thank Dr. Pierre Sarazin for fruitful discussions, Professor Patrick Desjardins from the Department of Engineering Physics for the use of the atomic force microscopy apparatus, and Professor Gilles L'Espérance from the Center for Characterization and Microscopy of Materials $(CM)^2$ for the use of the focused ion beam. N.V. acknowledges the Fonds Québecois de la Recherche sur la Nature et les Technologies (FQRNT) for a scholarship.

References and Notes

(1) Harkins, W. D.; Feldman, A. *J. Am. Chem. Soc.* **1922**, *44*, 2665–2685.
(2) Harkins, W. D. *J. Chem. Phys.* **1941**, *9*, 552–568.
(3) Torza, S.; Mason, S. G. *J. Colloid Interface Sci.* **1970**, *33*, 67–83.
(4) De Gennes, P.-G.; Brochard-Wyart, F.; Quéré, D. In *Capillarity and Wetting Phenomena - Drops, Bubbles, Pearls, Waves*; Springer Science: New York, 2004, p 15.
(5) Torza, S. *Interfacial Phenomena in Shear and Electrical Fields*. Ph.D. Thesis, McGill University: Montréal, Canada, 1969.
(6) Hobbs, S. Y.; Dekkers, M. E. J.; Watkins, V. H. *Polymer* **1988**, *29*, 1598–1602.
(7) Nemirovski, N.; Siegmann, A.; Narkis, M. *J. Macromol. Sci.—Phys.* **1995**, *B34*, 459–475.
(8) Guo, H. F.; Packirisamy, S.; Gvozdic, N. V.; Meier, D. J. *Polymer* **1997**, *38*, 785–794.
(9) Luzinov, I.; Xi, K.; Pagnoulle, C.; Huynh-Ba, G.; Jérôme, R. *Polymer* **1999**, *40*, 2511–2520.
(10) Hemmati, M.; Nazokdast, H.; Panahi, H. S. *J. Appl. Polym. Sci.* **2001**, *82*, 1129–1137.
(11) Reignier, J.; Favis, B. D. *AIChE J.* **2003**, *49*, 1014–1023.
(12) Reignier, J.; Favis, B. D.; Heuzey, M.-C. *Polymer* **2003**, *44*, 49–59.
(13) Reignier, J.; Favis, B. D. *Polymer* **2003**, *44*, 5061–5066.
(14) Reignier, J.; Favis, B. D. *Macromolecules* **2000**, *33*, 6998–7008.
(15) Omonov, T. S.; Harrats, C.; Groeninckx, G. *Polymer* **2005**, *46*, 12322–12336.
(16) Valera, T. S.; Morita, A. T.; Demarquette, N. R. *Macromolecules* **2006**, *39*, 2663–2675.
(17) Debolt, M. A.; Robertson, R. E. *Polym. Eng. Sci.* **2006**, *46*, 385–398.
(18) De Freitas, C. A.; Valera, T. S.; De Souza, A. M. C.; Demarquette, N. R. *Macromol. Symp.* **2007**, *247*, 260–270.
(19) Horiuchi, S.; Matchariyakul, N.; Yase, K.; Kitano, T. *Macromolecules* **1997**, *30*, 3664–3670.
(20) Van Oene, H. *J. Colloid Interface Sci.* **1972**, *40*, 448–467.
(21) Hyun, D. C.; Jeong, U.; Ryu, D. Y. *J. Polym. Sci., B: Polym. Phys.* **2007**, *45*, 2729–2738.
(22) Kim, J. K.; Jeong, W.-Y.; Son, J.-M.; Jeon, H. K. *Macromolecules* **2000**, *33*, 9161–9165.
(23) Zhang, X.; Kim, J. K. *Macromol. Rapid Commun.* **1998**, *19*, 499–504.
(24) Tomotika, S. *Proc. R. Soc. London A* **1934**, *A150*, 322–337.
(25) Utracki, L. A.; Shi, Z. H. *Polym. Eng. Sci.* **1992**, *32*, 1824–1833.
(26) Mekhilef, N.; Favis, B. D.; Carreau, P. J. *J. Polym. Sci., B: Polym. Phys.* **1997**, *35*, 293–308.
(27) Virgilio, N.; Desjardins, P.; Pépin, M.-F.; L'Espérance, G.; Favis, B. D. *Macromolecules* **2005**, *38*, 2368.
(28) Saltikov, S. A. *Proceedings of the 2nd International Congress for Stereology*; Helias: New York, 1967.
(29) Rowlinson J. S. and Widom B. *Molecular Theory of Capillarity*; Oxford University Press: Oxford, U.K., 1982; p 207.
(30) Chaffin, K. A.; Knutsen, J. S.; Brant, P.; Bates, F. S. *Science* **2000**, *288*, 2187–2190.
(31) Chaffin, K. A.; Bates, F. S.; Bryant, P.; Brown, G. M. *J. Polym. Sci., B: Polym. Phys.* **2000**, *38*, 108–121.
(32) Sauer, B. B.; Dee, G. T. *Macromolecules* **1991**, *24*, 2124–2126.
(33) Anastasiadis, S. H.; Gancarz, I.; Koberstein, J. T. *Macromolecules* **1988**, *21*, 2980–2987.
(34) Cigana, P.; Favis, B. D.; Jérôme, R. *J. Polym. Sci., B: Polym. Phys.* **1996**, *34*, 1691–1700.
(35) Cigana, P.; Favis, B. D. *Polymer* **1998**, *39*, 3373–3378.
(36) Macosko, C. W.; Guégan, P.; Khandpur, A.; Nakayama, A.; Maréchal, P.; Inoue, T. *Macromolecules* **1996**, *29*, 5590–5598.
(37) Adedeji, A.; Lyu, S.; Macosko, C. W. *Macromolecules* **2001**, *34*, 8663–8668.
(38) Polizu, S.; Favis, B. D.; Vu-Khanh, T. *Macromolecules* **1999**, *32*, 3448–3456.
(39) Li, J.; Favis, B. D. *Polymer* **2002**, *43*, 4935–4945.
(40) Pyun, A.; Bell, J. R.; Won, K. H.; Weon, B. M.; Seol, S. K.; Je, J. H.; Macosko, C. W. *Macromolecules* **2007**, *40*, 2029–2035.
(41) Omonov, T. S.; Harrats, C.; Groeninckx, G.; Moldenaers, P. *Polymer* **2007**, *48*, 5289–5302.
(42) Yuan, Z.; Favis, B. D. *J. Polym. Sci., B: Polym. Phys.* **2006**, *44*, 711–721.
(43) Galloway, J. A.; Jeon, H. K.; Bell, J. R.; Macosko, C. W. *Polymer* **2005**, *46*, 183–191.
(44) Sarazin, P.; Favis, B. D. *Biomacromolecules* **2003**, *4*, 1669–1679.
(45) Lyu, S.; Jones, T. D.; Bates, F. S.; Macosko, C. W. *Macromolecules* **2002**, *35*, 7845–7855.
(46) Sundararaj, U.; Macosko, C. W. *Macromolecules* **1995**, *28*, 2647–2657.
(47) Böker, A.; He, J.; Emrick, T.; Russell, T. P. *Soft Matter* **2007**, *3*, 1231–1248.
(48) Sacanna, S.; Kegel, W. K.; Philipse, A. P. *Phys. Rev. Lett.* **2007**, *98*, 158301.
(49) Arditty, S.; Schmitt, V.; Lequeux, F.; Leal-Calderon, F. *Eur. Phys. J. B* **2005**, *44*, 381–393.
(50) Kralchevsky, P. A.; Ivanov, I. B.; Ananthapadmanabhan, K. P.; Lips, A. *Langmuir* **2005**, *21*, 50–63.
(51) Arditty, S.; Whitby, C. P.; Binks, B. P.; Schmitt, V.; Leal-Calderon, F. *Eur. Phys. J. E* **2003**, *11*, 273–281.
(52) Aveyard, R.; Binks, B. P.; Clint, J. H. *Adv. Colloid Interface Sci.* **2003**, *100—102*, 503–546.
(53) Binks, B. P.; Lumsdon, S. O. *Langmuir* **2000**, *16*, 8622–8631.
(54) Whitesides, T. M.; Ross, D. S. *J. Colloid Interface Sci.* **1995**, *169*, 48–59.
(55) Cates, M. E.; Clegg, P. S. *Soft Matter* **2008**, *4*, 2132–2138.
(56) Stratford, K.; Adhikari, R.; Pagonabarraga, I.; Desplat, J.-C.; Cates, M. E. *Science* **2005**, *309*, 2198–2201.
(57) Vermant, J.; Cioccolo, G.; Golapan Nair, K.; Moldenaers, P. *Rheol. Acta* **2004**, *43*, 529–538.
(58) Mironi-Harpaz, I.; Narkis, M. *J. Appl. Polym. Sci.* **2001**, *81*, 104–115.
(59) Calberg, C.; Blacher, S.; Gubbels, F.; Brouers, F.; Deltour, R.; Jérôme, R. *J. Phys. D: Appl. Phys.* **1999**, *32*, 1517–1525.
(60) Gubbels, F.; Blacher, S.; Vanlathem, E.; Jérôme, R.; Deltour, R.; Brouers, F.; Teyssie, P. *Macromolecules* **1995**, *28*, 1559–1566.

MA802544Q